Carbohydrate Polymers 86 (2011) 708–715

Contents lists available at ScienceDirect

Carbohydrate Polymers

journal homepage: www.elsevier.com/locate/carbpol

Self-quenchable biofunctional nanoparticles of heparin–folate-photosensitizer conjugates for photodynamic therapy

Li Li[a,1], Byoung-chan Bae[b,1], Thanh Huyen Tran[a], Kwon Hyeok Yoon[a], Kun Na[b,*], Kang Moo Huh[a,*]

[a] Department of Polymer Science and Engineering, Chungnam National University, Daejeon 305-764, Republic of Korea
[b] Department of Biotechnology, The Catholic University of Korea, Bucheon 420-743, Republic of Korea

ARTICLE INFO

Article history:
Received 16 March 2011
Received in revised form 10 May 2011
Accepted 11 May 2011
Available online 19 May 2011

Keywords:
Heparin
Photosensitizer
Photodynamic therapy
Self-assembled nanoparticles
Drug delivery

ABSTRACT

Novel amphiphilic polysaccharide/PS conjugates synthesized by chemical conjugation of heparin with a hydrophobic photosensitizer (PS), pheophorbide a (PhA), and a targeting ligand, folate, were investigated for their potential application in photodynamic therapy (PDT). The anticoagulant activity of heparin-PhA (HP) and folate–heparin–PhA (FHP) conjugates was significantly decreased compared to that of heparin, thereby potentially reducing the hemorrhagic side effects. The critical self-quenching concentrations of the conjugates were decreased as the content of PhA rose. HP and FHP conjugates formed nano-sized particles in aqueous medium through a self-assembling process, and the nanoparticles were 130–170 nm in size, with a unimodal pattern of size distribution. Photoactivity of HP and FHP nanoparticles was evaluated by measuring the generation of singlet oxygen in DMF and PBS. The nanoparticles displayed a self-photoquenching effect in PBS, while the generation of singlet oxygen dramatically increased in DMF. HP and FHP nanoparticles exhibited marked phototoxicity on HeLa cells and were minimally dark-toxic without light treatment.

1. Introduction

Photodynamic therapy (PDT) is a protocol that uses photosensitizers (PSs) and light in the presence of oxygen to cause selective damage to a target tissue (Dolmans, Fukumura & Jain, 2003). Because PSs are typically harmless without light, tumor site treatment can be precisely targeted by selective illumination, limiting the damage to surrounding healthy tissues. Pheophorbide a (PhA), a second generation PS, is an anionic porphyrin derivative that can be easily prepared from chlorophyll. Its antitumor effect when used as a PDT agent on a number of human cancer cell types, including colonic cancer cells (Hajri et al., 2002), uterine carcinoma cells (Tang, Liu, Zhang, Fong & Fung, 2009), hepatic carcinoma cells (Tang et al., 2006), and human lung cancer cells (Yin, Zhou, Jie, Xing & Zhang, 2004) has been reported. It is known that PhA has a high extinction coefficient in the red region of the spectrum. This provides an advantage over porphyrins used in PDT, where longer wavelength lasers are used for better penetration into tissues. In addition, its relatively fast elimination from the body may shorten side effects caused by long-lasting cutaneous photosensitivity (Roder, Hanke, Oelckers, Hackbarth & Symietz, 2000). However, the intravenous use of PhA is greatly hampered by its limited solubility in aqueous media. Therefore, the formulation of an injectable PhA product with satisfactory solubility in aqueous solutions is of great interest for PDT.

The formulation of hydrophobic PS using a nanoparticulate drug delivery system is an attractive strategy (Bechet et al., 2008). Nano-drug carriers may not only enhance the solubility of hydrophobic PS, but also enable the incorporated drugs to be passively transported and targeted to the tumor site through the enhanced permeability and retention (EPR) effect. Furthermore, the presence of active targeting molecules on the nanoparticle surface can further enhance the therapeutic efficacy and reduce the side effects of hydrophobic PDT agents, while achieving desired effects and a greater uptake of the nanoparticles by tumor cells (Allison, Mota, Bagnato & Sibata, 2008; Konan, Gurny & Allemann, 2002).

Among various biomaterials, natural polysaccharides seem to be the most promising materials for the preparation of nano-PS carriers due to their outstanding merits (Liu, Jiao, Wang, Zhou & Zhang, 2008), such as high water solubility, good biocompatibility, a wide range of molecular weights, and an abundance of sources. In recent studies, polysaccharides have been popularly used for the formulation of hydrophobic PSs, such as protoporphyrin IX encapsulated glycol chitosan-based nanoparticles (Lee et al., 2009), acetylated hyaluronic acid/PhA conjugates (Li, Bae, & Na, 2010; Li, Huh, Lee, & Kim, 2010), and pullulan/folate-PhA conjugates (Bae & Na, 2010). These PS formulations showed great potential for application in PDT.

* Corresponding authors. Tel.: +82 42 821 6663; fax: +82 42 821 8910.
E-mail addresses: kna6997@catholic.ac.kr (K. Na), khuh@cnu.ac.kr (K.M. Huh).
[1] These authors contributed equally to this work.

0144-8617/$ – see front matter © 2011 Elsevier Ltd. All rights reserved.
doi:10.1016/j.carbpol.2011.05.011

In this study, we developed a new amphiphilic polysaccharide/PS conjugate by chemical conjugation of heparin with hydrophobic PhA and a targeting ligand, folate. Heparin, a highly sulfated polysaccharide belonging to the family of glycosaminoglycans, has numerous important biological activities associated with its interaction with diverse proteins, such as anticoagulant activity (Linhardt, 1991), and inhibition of VEGF- and bFGF-mediated tumor angiogenesis (Mousa & Petersen, 2009), tumor metastasis (Bobek & Kovarik, 2004), and proliferation of arterial smooth muscle cells (Smorenburg & Van Noorden, 2001). Recently, conjugates of heparin with hydrophobic anticancer agents or low molecular weight molecules have been widely investigated as antitumor drugs and drug carriers (Cho, Moon, Park, Jeon, Byun & Lee, 2008; Park et al., 2006; Park, Kim, Tran, Huh & Lee, 2010; Park, Tran, et al.2010). However, the conjugation of PS with heparin for use in actively targeted PDT has not been reported.

Here, we report the syntheses and characterizations of heparin-PhA (HP), and folate–heparin–PhA (FHP) conjugates. The anticoagulant activities and the critical self-quenching concentrations (CQCs) of conjugates were studied. Physicochemical properties, such as particle size and zeta potential, were also examined. The photoactivity of HP and FHP nanoparticles, as well as their in vitro phototoxicities on HeLa cells, was also investigated.

2. Experimental

2.1. Materials

Heparin (Fraxiparin®), with an average molecular weight of 6000 Da, was obtained from Mediplex Co. (Korea). Pheophorbide, a (PhA), was purchased from Frontier Scientific Inc. (Logan, UT, USA). Folate, ethylenediamine, N,N′-dicyclohexylcarbodiimide (DCC), N-hydroxysuccinimide (NHS), 1-ethyl-3-(3-dimethylaminopropyl) carbodiimide hydrochloride (EDC), 9,10-dimethylanthracene (DMA), and pyrene were purchased from Sigma–Aldrich Chemical Co. (St. Louis, MO, USA). Spectra/Por membranes were purchased from Spectrum Laboratories, Inc. (Rancho Dominguez, CA, USA and Canada). RPMI 1640 medium, Dulbecco's modified Eagle's medium (DMEM), fetal bovine serum (FBS), antibiotics (penicillin and streptomycin), and Dulbecco's phosphate buffered saline (DPBS) were obtained from GibcoBRL (Invitrogen Corp., Carlsbad, CA, USA). All chemicals were analytical grade and used as received without further purification.

2.2. Synthesis of heparin–PhA (HP) and folate–heparin–PhA (FHP) conjugates

2.2.1. Preparation of aminated folate

The synthetic method for aminated folate was previously reported elsewhere (Li, Bae, et al., 2010; Li, Huh, et al., 2010). Briefly, folate (441 mg) dissolved in 20 mL of dimethyl sulfoxide (DMSO) was activated with DCC (248 mg) and NHS (230 mg) at room temperature for 12 h. The by-product, dicyclohexylurea (DCU), was removed by filtration. The resulting activated folate-NHS was reacted with ethylenediamine (0.67 mL) and pyridine (100 μL) at room temperature for an additional 12 h. The aminated folate was precipitated with an excess of acetonitrile and washed three times with diethyl ether. The yellow powder was obtained after drying under vacuum (Fig. 1a).

2.2.2. Preparation of aminated PhA

PhA (160 mg) was activated with EDC (61.6 mg) and NHS (61.6 mg) in 10 mL of dimethylformamide (DMF) at room temperature for 12 h, and then ethylenediamine (36 μL) and pyridine (20 μL) were added. After a 12 h reaction, the solution was dialyzed for 2 days against deionized water to remove the byproducts, organic solvent, and unreacted compounds. The dark green powder was obtained after ultracentrifugation and freeze-drying (Fig. 1b).

2.2.3. Synthesis of HP and FHP conjugates

HP was synthesized by coupling aminated PhA with heparin through amide covalent bonds using EDC as a coupling agent. In brief, heparin (50 mg) was dissolved in 5 mL of formamide by gentle heating. EDC (24.8 mg, in excess) was added to the heparin solution, followed by mixing with aminated PhA in DMF (5 mL). The feed ratios of aminated PhA to heparin are listed in Table 1. The reaction was carried out at room temperature for 36 h under nitrogen gas. After the coupling reaction, the reacted solution was dialyzed for 3 days to remove low molecular agents. The crude products were obtained after freeze-drying, and then washed with methanol to remove uncoupled aminated PhA. The final products were collected by centrifugation, and dried under vacuum. For the synthesis of FHP conjugates, the heparin solution and aminated PhA solution were prepared first, and then EDC and aminated folate were added to the heparin solution, followed by mixing with aminated PhA. The one-step reaction for FHP and the purification steps were conducted as those used for HP conjugates (Fig. 1c). The synthesized HP and FHP conjugates were analyzed by ^{1}H NMR spectroscopy (Bruker, Germany).

2.3. Characterization of HP and FHP conjugates

The coupling ratios of PhA and folate on the heparin backbone were determined by a colorimetric method. Briefly, the lyophilized HP or FHP was dissolved in 10 mL formamide to obtain a clear solution. The absorbance at 290 nm and 669 nm was read with a UV-VIS spectrophotometer (Mini-1024, SHIMADZU, Japan). The content of PhA and folate conjugated to heparin was calculated based on a calibration curve of PhA (669 nm) and folate (290 nm) in formamide, respectively.

The anticoagulant activities of HP and FHP conjugates were determined by the FXa chromogenic assay that was described in detail in our previous report (Li et al., 2011).

2.4. Measurement of the critical self-quenching concentration (CQC)

The CQCs of HP and FHP conjugates were determined using pyrene fluorescence spectroscopy, as described in the literature (Bae & Na, 2010) with minimal modification. Briefly, pyrene solution in tetrahydrofuran (THF) (0.5 mg/mL) was added to 2 L of dionized water in such an amount that the final concentration of pyrene in water was 6.0×10^{-7} M. THF was removed by distillation at 70 °C for 3 h with vigorous stirring. HP and FHP solutions with various concentrations were prepared and mixed with pyrene solution. The final concentrations of HP and FHP conjugates in the mixture ranged from 0.05 mg/L to 200 mg/L, which included a trace of pyrene (3.0×10^{-7} M) in each vial. Fluorescence measurements were performed at room temperature using a Jasco Model FP6500 spectrofluorometer (Japan). The slit widths were fixed at 10 nm. Fluorescence excitation spectra of pyrene were recorded using an emission wavelength of 390.0 nm.

2.5. Preparation and characterization of self-assembled HP and FHP nanoparticles

The HP and FHP nanoparticles were prepared by a dialysis method. HP or FHP conjugates (5 mg) were dissolved in 5 mL of formamide, followed by sonication for 10 min to obtain a clear solution. The solution was dialyzed against deionized water for 2 days. After filtration with a 0.45 μm syringe filter, the average particle size, size distribution, and zeta-potential of each sample

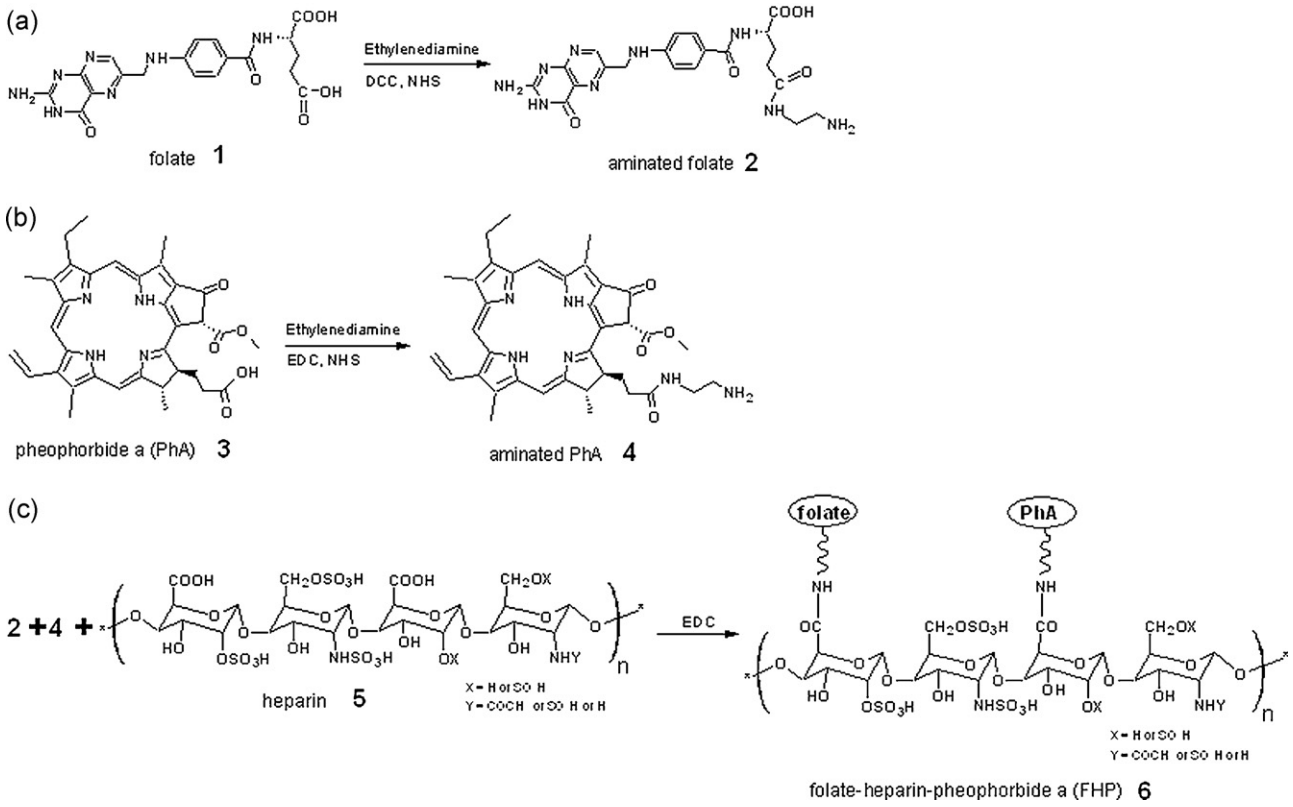

Fig. 1. Schematic diagram of the synthesis of (a) aminated folate, (b) aminated PhA, and (c) FHP.

were measured using a dynamic light scattering instrument (ELS-Z series, Otsuka Electronics, Japan). The morphology of HP and FHP nanoparticles was observed by a field emission scanning electron microscope (FE-SEM; JSM-7000F, JEOL, Japan) at 15 kV.

2.6. Observation of self-quenching effects of HP and FHP nanoparticles

To monitor changes of fluorescence in different solvents, HP and FHP nanoparticles were dissolved in PBS and DMF in EP-tubes, respectively. Fluorescence images were detected with a KODAK Image Station after being dissolved in different solvents. Images were obtained using a 12-bit CCD camera (Image Station 4000 MM; Kodak, New Haven, CT, USA) equipped with a special C-mount lens and a long wave emission filter (600–700 nm; Omega Optical, Brattleboro, VT, USA).

2.7. Determination of singlet oxygen generation

The generation of singlet oxygen can be measured by the decrease of fluorescence intensity of 9,10-dimethylanthracene (DMA), utilizing fluorescent spectroscopy as an independent method. The standard stock solution of DMA in DMF was stored in the dark at 4 °C until use, at which time it was diluted to a final concentration of 1.184×10^{-5} M with DMF or PBS buffer. HP and FHP nanoparticles (PhA, 1.5 μg/mL) were also dissolved in DMF or PBS buffer (pH 7.4) and added to DMA. The mixtures were irradiated at a light intensity of 3 mW/cm^2 using a 670 nm laser source (Institute of Electronics, The Catholic University of Korea). A collimated laser beam was directed at the sample cuvette through an optical fiber. The decrease in fluorescence intensity of DMA (emission 380–550 nm, with excitation at 360 nm) as a result of singlet oxygen generation was monitored using a spectrofluoro photometer controlled by a PC. Singlet oxygen quantum yield was calculated by the following equation (Hoebeke & Damoiseau, 2002):

$$\Phi_\Delta = \frac{k_S}{k_R} \times \frac{A_R}{A_S} \times \text{ref.}\Phi_\Delta$$

where A is absorbance at 670 nm (the excitation wave length), k is the gradient of the absorbance curve, S refers to the sample, and R to the reference. SOQ (Φ_Δ) of each sample was calculated from the reference Φ_Δ value (PhA 0.52: ref. Φ_Δ) (Fernandez, Bilgin & Grossweiner, 1997; Roslaniec, Weitman, Freeman, Mazur & Ehrenberg, 2000).

Table 1
Characterization of HP and FHP conjugates.

Sample	Feed molar ratio (folate:heparin:PhA)	Coupling ratio (folate:heparin:PhA)	CQC[a] (mg/L)	Size (nm)	Zeta-potential (mV)	Anticoagulant activity[b] (IU/mg)	SOQ in DMF[c]
HP1	–:1:6	–:1:4.67	1.73	174.1 ± 3.2	−33.59 ± 0.34	71.7	0.47
HP2	–:1:10	–:1:7.24	0.39	134.6 ± 1.5	−30.70 ± 0.55	51.6	0.47
FHP1	5:1:6	3.04:1:4.14	4.90	167.0 ± 1.7	−20.62 ± 1.02	55.4	0.48
FHP2	5:1:10	2.67:1:6.71	1.08	145.2 ± 3.0	−20.44 ± 0.78	40.2	0.47

[a] CQC (critical self-quenching concentration).
[b] The anticoagulant activity of heparin is 101 IU/mg.
[c] SOQ (singlet oxygen quantum yield (Φ_Δ)): In DMF (PhA, 0.52).

2.8. Cell cytotoxicity of HP and FHP nanoparticles

HeLa cells (5×10^4 per well) were seeded on 96-well plates and cultured in 200 μL culture medium for 1 day. After incubation for 12 h with different concentrations of HP, FHP nanoparticles and free PhA (0.0015–1.5 μg/mL of Pheo-A), the medium was replaced with fresh RPMI 1640 just prior to irradiation at 1.2 J/cm^2 by a 670 nm laser source (Institute of Electronics). After 24 h of incubation, phototoxicity and dark-toxicity were determined using 3-[4,5-dim ethylthiazol-2-yl]-3,5-diphenyltetrazolium bromide dye (MTT dye, 2 mg/mL) uptake at 570 nm on an ELISA reader.

3. Results and discussion

3.1. Synthesis and characterization of HP and FHP conjugates

To our knowledge, among a variety of polysaccharides, heparin is the unique polymer that possesses anti-cancer activities. Several preclinical studies have indicated that heparin has a marked effect on VEGF- and bFGF-mediated tumor angiogenesis, as well as an inhibitory effect on tumor metastasis through interference with endothelial cell adhesion (Bobek & Kovarik, 2004; Mousa & Petersen, 2009; Smorenburg & Van Noorden, 2001). PDT is a local treatment and generally cannot be used to treat cancer that has spread (metastasized) (MacDonald & Dougherty, 2001). Heparin could be used as a nanocarrier in PDT, used in combination with antiangiogenic therapy, to enhance the response to PDT during cancer treatment (Dolmans et al., 2003; Ferrario et al., 2000). Here, we synthesized amphiphilic HP conjugates by conjugating hydrophobic PhA to hydrophilic heparin. Folate conjugated HP was synthesized for binding the folate-receptor in tumor cells during actively targeted PDT. Aminated folate and PhA were initially prepared by covalent bonding of the carboxyl group of folate and PhA with ethylenediamine using DCC/NHS and EDC/NHS as coupling agents, respectively (Fig. 1a and b). HP conjugates, with or without folate conjugation, were then synthesized by a simple one-step reaction of the amino groups of PhA and folate with the carboxylic groups of heparin (Fig. 1c). The chemical compositions of HP and FHP conjugates were confirmed by ^{1}H NMR measurements. The characteristic chemical shifts of HP conjugates corresponding to heparin (3.9, 4.0 ppm) (Fig. 2a), and aminated PhA (4.6, 5.9, 6.4–6.5, 8.9, 9.4, 9.7–9.8 ppm) (Fig. 2c) were observed in the ^{1}H NMR spectrum of HP (Fig. 2d). Besides the characteristic peaks of heparin and PhA, the typical peaks of aminated folate were observed at 4.5, 6.7, 6.9, and 8.6 ppm in the ^{1}H NMR spectrum of FHP (Fig. 2e).

HP conjugates with different PhA contents were prepared by varying the feed molar ratios of PhA to heparin (Table 1). The coupling ratios of PhA increased from 4.67 to 7.24, corresponding to PhA feed molar ratios of 6 and 10, respectively. For FHP conjugates, the feed molar ratio of folate/heparin was fixed at 5/1. The coupling ratios of folate and PhA for FHP1 were 3.04 and 4.14, and for FHP2 they were 2.67 and 6.71, respectively. The coupling ratios of folate in FHP1 and FHP2 were similar to each other, while the coupling ratio of PhA to the heparin backbone increased with increasing the PhA feed molar ratio, indicating that the coupling reaction of PhA/heparin was not as significantly affected by the presence of folate moieties. Therefore, the one-step reaction method for preparing the FHP conjugates can be considered as a feasible and simple way to introduce the folate ligands and PhA to the heparin backbone.

As shown in Table 1, the anticoagulant activities of HP and FHP conjugates ranged from 40.2 to 71.7 IU/mg, which were significantly lower than that of unmodified heparin (101 IU/mg). The anticoagulant activity decreased according to the increase in the amount of chemically coupled PhA and folate moieties. The conjugation of PhA and folate to the heparin backbone resulted in lower anticoagulant activity of heparin, because the carboxyl groups of heparin, which play an important role in anticoagulant activity, were modified by conjugation. However, HP and FHP conjugates may retain their antitumor efficacy because the sulfate groups, which are important for endothelial cell binding or inhibition of VEGF- and bFGF-mediated angiogenesis, are left unaltered (Barzu et al., 1986). The application of heparin as an anticancer agent is limited by its high anticoagulant activity, because the administration of heparin may induce serious side effects, such as hemorrhage, thrombocytopenia, and osteoporosis. Thus, HP and FHP conjugates with reduced anticoagulant activity could be safe for long term delivery of PhA during PDT.

3.2. Critical self-quenching concentrations (CQCs) of HP and FHP conjugates

In general, the critical micelle concentration (CMC) or critical aggregation concentration (CAC) of amphiphiles is determined using the pyrene fluorescence probe method. At values below the CMC or CAC, pyrene is soluble in polar aqueous solution. When micelles are formed, pyrene may preferentially partition into the hydrophobic domain formed by a micellar core. As a medium of high polarity changes to a non-polar environment, numerous changes in the pyrene fluorescence spectra can be observed, including an increase in the fluorescence intensity and a red shift of the (0,0) band in the excitation spectra (Kalyanasundaram & Thomas, 1977). When HP and FHP conjugates spontaneously form nanoparticles, pyrene also preferentially partitions toward the hydrophobic PhA core. However, probably due to the strong quenching effect of the hydrophobic interaction between PhA and pyrene, known as the fluorescence resonance energy transfer effect induced by the aggregation behavior of PhA and π–π stacking interactions, a decrease of pyrene fluorescence intensity was observed (Fig. 3a). Based on this special change, Li, Bae, et al. (2010) and Li, Huh, et al. (2010) proposed a new term (CQC) to describe the threshold concentration of polysaccharide-PS amphiphiles required to quench the fluorescence of pyrene. A similar phenomenon was observed in the study by Bae and Na (2010) where the pyrene fluorescence intensity at 335 nm decreased, with an increase in the concentration of folate–pullulan–PhA conjugates, and a red shift of (0,0) was not observed following the addition of the polymer. Fig. 3b shows a plot of the fluorescence intensity of pyrene at 335 nm vs. the concentration of FHP2; a major change in the slope indicates the onset of self-quenching. As shown in Table 1, the CQCs of HP and FHP conjugates were in the range of 0.39–4.90 mg/L, which decreased with increasing content of PhA, indicating that a higher hydrophobic PhA content enabled the conjugates to spontaneously form nanoparticles at a lower concentration. Nevertheless, the presence of folate ligands did not show a significant effect on CQCs of HP conjugates at a nearly similar PhA content. The CQCs of FHP1 and HP1 were 4.90 mg/L and 1.73 mg/L, respectively, when the coupling ratios of PhA were 4.14 and 4.67, respectively, indicating that the CQC values of HP and FHP conjugates were highly dependent on the core forming component, PhA. The CQC values of HP and FHP conjugates were significantly lower than those of folate–pullulan–PhA conjugates (0.08–0.27 g/L) (Bae & Na, 2010), and acetylated hyaluronic acid–PhA conjugates (0.26–2.10 M) (Li, Bae, et al., 2010; Li, Huh, et al., 2010). Because the intravenous injection of nanoparticle solutions is associated with extreme dilution by circulating blood, the low CQC values suggest that the HP and FHP nanoparticles are more favorable for systemic PhA delivery.

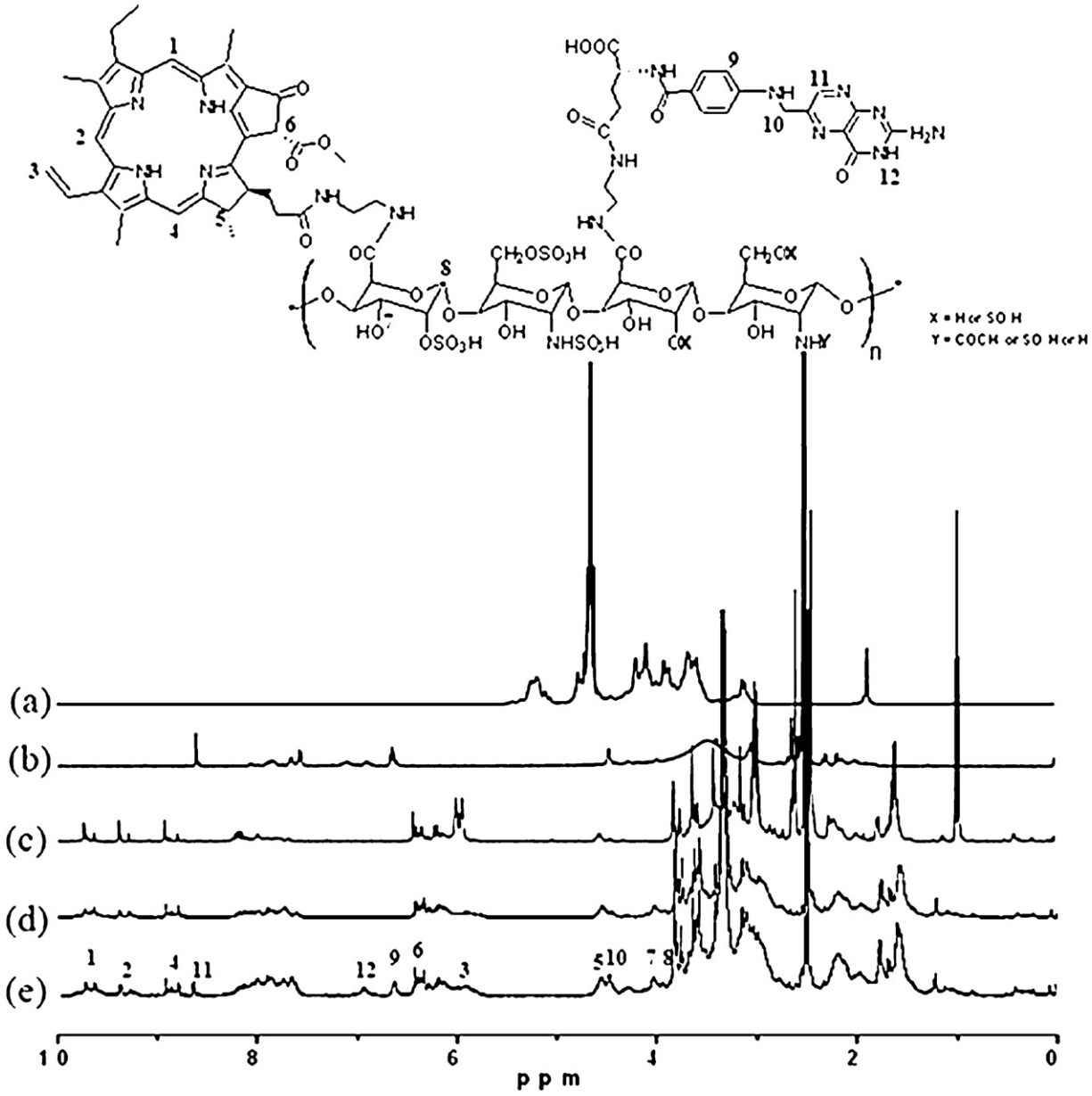

Fig. 2. ^{1}H NMR spectra of (a) heparin, (b) aminated folate, (c) aminated PhA, (d) HP, and (e) FHP.

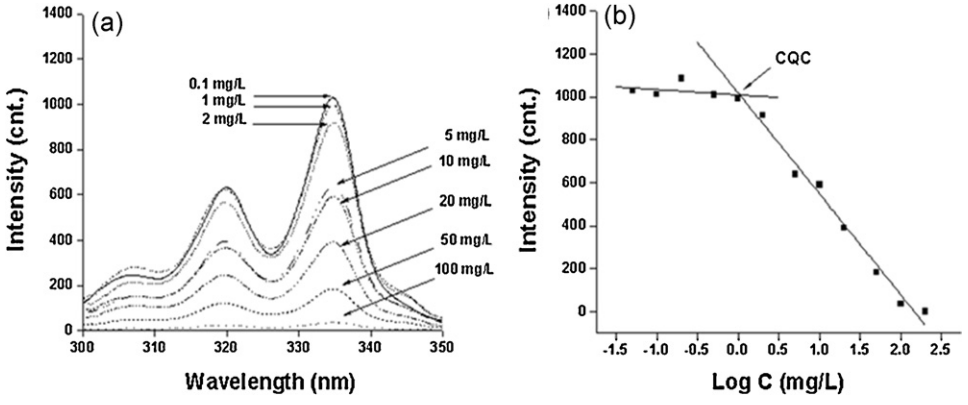

Fig. 3. CQC measurement of FHP: (a) excitation spectra of pyrene in FHP2 conjugate, and (b) the plot of the fluorescence intensity of pyrene at 335 nm against concentration of FHP2.

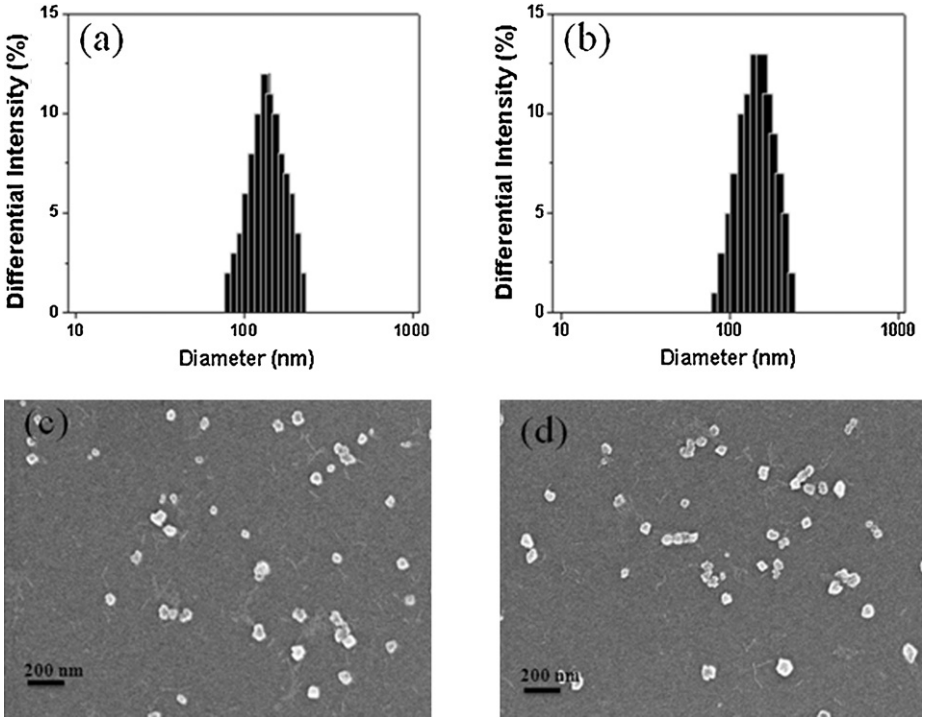

Fig. 4. Size distribution of HP and FHP, measured by DLS: (a) HP2 and (b) FHP2; and morphology of HP and FHP, measured by FE-SEM: (c) HP2 and (d) FHP2.

3.3. Characterization of HP and FHP self-assembled nanoparticles

HP and FHP conjugates readily self-assembled in aqueous solutions to form nanoparticles by a dialysis process. The driving force of their self-assembling behavior is due to the hydrophobic interaction between conjugated PhA moieties. The nanoparticles may have a core–shell structure with a hydrophobic PhA inner core surrounded by a hydrophilic outer shell of heparin or heparin–folate. The average particle size of HP and FHP nanoparticles ranged from 134.6 to 174.1 nm (Table 1), which decreased with increasing PhA coupling ratio, due to the formation of a more compact hydrophobic inner core. However, the conjugation of folate ligand did not induce a significant change in the particle size of HP and FHP nanoparticles. For example, the particle sizes of HP1 and FHP1 were 174.1 nm and 167.0 nm, respectively, at a similar coupling ratio for PhA (4.67 for HP1 and 4.14 for FHP1, respectively). The size distribution of HP and FHP nanoparticles, measured by DLS, showed a unimodal pattern (Fig. 4a and b). The FE-SEM images showed spherical HP2 and FHP2 nanoparticles with a diameter of 80–100 nm, which was ~30–40 nm smaller than the size determined by DLS (Fig. 4c and d). The particle size determined by DLS measurement reflected the hydrodynamic diameter of the micelle structure, which was swollen in aqueous solution, while FE-SEM observed the size of nanoparticles in the dried state. It is known that the large gaps (400–800 nm) between the endothelial cells in the microvasculature of solid tumors enable nanoparticles to preferentially accumulate and reside in the tumor mass via the EPR effect (Matsumura & Maeda, 1986). Therefore, HP and FHP nanoparticles with small size (<200 nm) are considered to be suitable for the accumulation of PhA at the targeted tumor through the EPR effect. The HP and FHP nanoparticles were negatively charged at their surface, as reflected in the zeta-potential values (−20.44–33.59 mV) (Table 1), indicating that negatively charged heparin covers the self-assembled nanoparticles. FHP nanoparticles showed fewer negative charges than HP nanoparticles, which may be because conjugated folate molecules partially shielded the surface areas of negatively charged heparin outer shells, and more negative carboxyl groups were chemically modified via the coupling reaction. This negative surface charge may cause HP and FHP nanoparticles to possess long-term colloidal stability in a physiological environment.

3.4. Photoactivity and determination of singlet oxygen production of HP and FHP nanoparticles

The photoactivity of free PhA, HP and FHP nanoparticles was determined by KODAK Image Station. Fig. 5 shows the near-infra red fluorescence (NIRF) images of free PhA, HP1, and FHP1 nanoparticles at a similar PhA concentration in DMF (red arrow) or PBS (blue arrow). Due to the FRET effect induced by the aggregation behavior of PhA via hydrophobic and π–π stacking interactions, the NIRF emissions of free PhA, HP, and FHP nanoparticles were obscure in lipophobic (PBS) solvent. Contrasting NIRF images were observed when free PhA, HP, and FHP nanoparticles were dissolved in lipophilic (DMF) solvent. The results implied the self-photoquenching potential of the HP and FHP nanoparticles.

To further prove the self-quenching effect of HP and FHP nanoparticles, the generation of singlet oxygen by HP and FHP

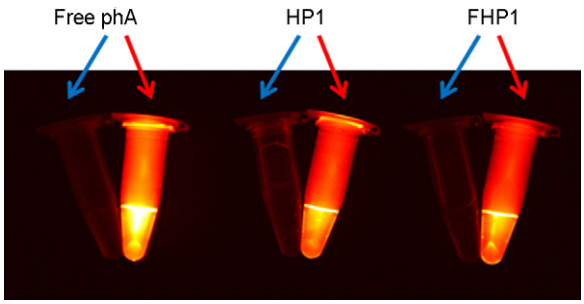

Fig. 5. Bright and NIRF image of HP, FHP nanoparticles and PhA (blue arrow: in PBS, red arrow: in DMF). (For interpretation of the references to color in this figure legend, the reader is referred to the web version of the article.)

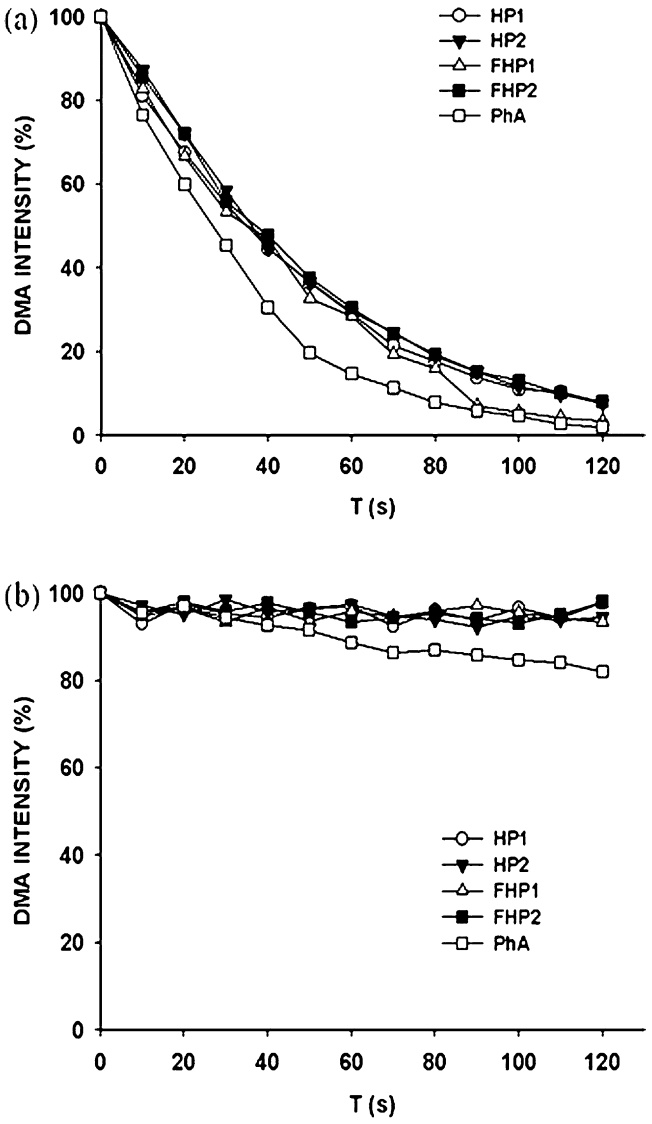

Fig. 6. Change in DMA fluorescence due to generation of singlet oxygen by HP, FHP nanoparticles and free PhA (a) in DMF and (b) in PBS.

nanoparticles in DMF and PBS, which governs the phototoxicity, was determined by calculating the singlet oxygen quantum yield, using DMA as the singlet oxygen trap. As shown in Fig. 6a, all samples produced a sharp decline in DMA fluorescent intensity, indicating the rapid generation of singlet oxygen upon laser irradiation when free PhA, HP, and FHP nanoparticles were dissolved in DMF. Singlet oxygen quantum yields (Φ_{Δ}) of HP1, HP2, FHP1, and FHP2 were calculated as 0.47, 0.47, 0.48, and 0.47, respectively, by a comparison of the slope for conjugates with the corresponding slope for free PhA ($\Phi = 0.52$). However, singlet oxygen generation was significantly changed in PBS (Fig. 6b). The generation of singlet oxygen dramatically decreased in PBS, according to the aggregation of PhA, showing the quenching effect. That result implied the HP and FHP nanoparticles could not be activated into the triplet state by mutual energy transfer, resulting in a decline of the ability to generate $^1O_2$.

The self-quenching effect of the PS-conjugated nanoparticles is advantageous for improving the therapeutic efficiency and lowering the side effects of PDT, such as skin photosensitivity. Physical incorporation of PS into polymeric nanocarrier systems is a conventional method to improve the solubility of hydrophobic PS, and

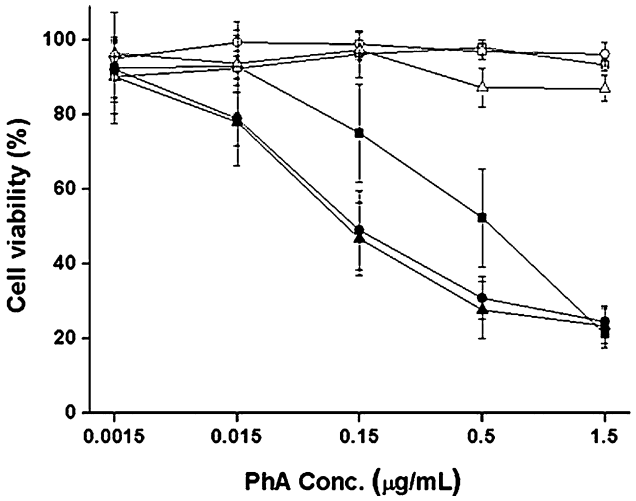

Fig. 7. Viability of HeLa cells determined by MTT assay after treat ment of HP1, FHP1 nanoparticles and PhA for 12 h: dark-toxicity ((○) HP1, (△) FHP1, (□) PhA) and phototoxicity ((●) HP1, (▲) FHP1, (■) PhA).

the incorporated PS may also have a self-photoquenching potential, due to the aggregation of PS at the inner core. However, during circulation in the blood, the physical-loading system cannot control phototoxicity caused by the inadvertent leakage of PS from the system, which leads to damage of normal tissue and blood cells. Therefore, the use of PS-conjugated nanoparticles with a self-quenching effect is a preferable system to switch phototoxicity during PDT: during circulation, the phototoxicity of PS can be completely suppressed until it reaches the target site, where the suppression can be rapidly reversed by environmental conditions such as pH, temperature, and enzymatic activity. Thus, the nanoparticles with self-quenchable photoactivity based on HP and FHP conjugates not only enhance the solubility of the hydrophobic PhA, but also minimize the unfavorable phototoxicity in PDT.

3.5. Phototoxicity of HP and FHP nanoparticles

To estimate the PDT efficacy of HP and FHP nanoparticles, the in vitro phototoxicity of the HP1 and FHP1 nanoparticles, as well as free PhA, on HeLa cells was compared after treatment with or without light at a dose of 1.2 J/cm^2 at 670 nm, as shown in Fig. 7. Without light treatment, free PhA, HP1, and FHP1 nanoparticles displayed a slight dark-toxicity (cell viability: 87.1–99.3%) in the range of 0.0015–1.5 μg/mL. However, following light treatment, both the HP1, and FHP1 nanoparticles, and free PhA showed significantly enhanced cytotoxicity, implying that the PhA containing nanoparticles effectively generated the cytotoxic species and induced the cell depletion. Although the photoactivity was suppressed in aqueous medium due to photoquenching, the phototoxicity of HP and FHP nanoparticles on living cells was maintained, which was probably due to a loss of the quenching effect by enzymatic attack within cellular compartments. When nanoparticles are internalized in cancer cells, a series of biological activities could induce the decomposition of the heparin backbone (Ernst, Langer, Cooney & Sasisekharan, 1995; Thunberg, Backstrom, Wasteson, Robinson, Ogren & Lindahl, 1982) and the cleavage of the amide bond between PhA and heparin; these interactions are involved in dissociation of aggregated PhA, and thus photoactivity could be restored due to loss of the quenching effect. Importantly, the phototoxicity of HP1 and FHP1 nanoparticles was higher than that of free PhA (IC50; HP: 0.15 μg/mL; FHP: 0.14 μg/mL; PhA: 0.4 μg/mL). The relatively greater phototoxicity of HP and FHP nanoparticles compared to free PhA may be related to not only the different cellular uptake

and localization characteristics of nanoparticles that leads to more efficient intracellular PhA localization via the endocytic pathway, but also reduced photoactivity of free PhA by possible negative aggregation behavior resulting in quenching effect in an aqueous environment. Therefore, the HP and FHP nanoparticles could be efficient carriers for the targeted delivery of PhA, with minimal side effects.

4. Conclusions

Self-assembled nanoparticles based on HP and FHP conjugates were prepared as potential PS carriers for use in PDT. The conjugation of PhA and folate molecules significantly lowered the anticoagulant activity of heparin. In aqueous media, HP and FHP conjugates formed self-assembled nanoparticles with a diameter <200 nm. The low CQC values (0.39–4.90 mg/L) suggest that the HP and FHP nanoparticles are stable for systemic PhA delivery. The results from photoactivity tests and a determination of singlet oxygen quantum yield, indicated the autoquenching properties of HP and FHP nanoparticles. The cytotoxicity of HP and FHP nanoparticles was higher than that of free PhA with light treatment, while the nanoparticles revealed low cytotoxicity against cancer cells without light. These findings indicated that the HP and FHP nanoparticles could be efficient carriers with practical applications in PDT.

Acknowledgements

This work was supported by a grant from the Fundamental R&D Program for Core Technology of Materials funded by the Ministry of Knowledge Economy, Republic of Korea.

References

Allison, R. R., Mota, H. C., Bagnato, V. S., & Sibata, C. H. (2008). Bio-nanotechnology and photodynamic therapy - State of the art review. *Photodiagnosis and Photodynamic Therapy*, *5*(1), 19–28.

Bae, B. C., & Na, K. (2010). Self-quenching polysaccharide-based nanogels of pullulan/folate-photosensitizer conjugates for photodynamic therapy. *Biomaterials*, *31*(24), 6325–6335.

Barzu, T., Van Rijn, J. L., Petitou, M., Molho, P., Tobelem, G., & Caen, J. P. (1986). Endothelial binding sites for heparin. Specificity and role in heparin neutralization. *Biochemistry Journal*, *238*(3), 847–854.

Bechet, D., Couleaud, P., Frochot, C., Viriot, M. L., Guillemin, F., & Barberi-Heyob, M. (2008). Nanoparticles as vehicles for delivery of photodynamic therapy agents. *Trends in Biotechnology*, *26*(11), 612–621.

Bobek, V., & Kovarik, J. (2004). Antitumor and antimetastatic effect of warfarin and heparins. *Biomedicine & Pharmacotherapy*, *58*(4), 213–219.

Cho, K. J., Moon, H. T., Park, G. E., Jeon, O. C., Byun, Y., & Lee, Y. K. (2008). Preparation of sodium deoxycholate (DOC) conjugated heparin derivatives for inhibition of angiogenesis and cancer cell growth. *Bioconjugate Chemistry*, *19*(7), 1346–1351.

Dolmans, D. E., Fukumura, D., & Jain, R. K. (2003). Photodynamic therapy for cancer. *Nature Reviews Cancer*, *3*(5), 380–387.

Ernst, S., Langer, R., Cooney, C. L., & Sasisekharan, R. (1995). Enzymatic degradation of glycosaminoglycans. *Critical Reviews in Biochemistry and Molecular Biology*, *30*(5), 387–444.

Fernandez, J. M., Bilgin, M. D., & Grossweiner, L. I. (1997). Singlet oxygen generation by photodynamic agents. *Journal of Photochemistry and Photobiology B-Biology*, *37*(1–2), 131–140.

Ferrario, A., von Tiehl, K. F., Rucker, N., Schwarz, M. A., Gill, P. S., & Gomer, C. J. (2000). Antiangiogenic treatment enhances photodynamic therapy responsiveness in a mouse mammary carcinoma. *Cancer Research*, *60*(15), 4066–4069.

Hajri, A., Wack, S., Meyer, C., Smith, M. K., Leberquier, C., Kedinger, M., & Aprahamian, M. (2002). In vitro and in vivo efficacy of photofrin and pheophorbide a, a bacteriochlorin, in photodynamic therapy of colonic cancer cells. *Photochemistry and Photobiology*, *75*(2), 140–148.

Hoebeke, M., & Damoiseau, X. (2002). Determination of the singlet oxygen quantum yield of bacteriochlorin a: A comparative study in phosphate buffer and aqueous dispersion of dimiristoyl-L-alpha-phosphatidylcholine liposomes. *Photochemistry and Photobiology Science*, *1*(4), 283–287.

Kalyanasundaram, K., & Thomas, J. K. (1977). Environmental effects on vibronic band intensities in pyrene monomer fluorescence and their application in studies of micellar systems. *Journal of the American Chemical Society*, *99*(7), 2039–2044.

Konan, Y. N., Gurny, R., & Allemann, E. (2002). State of the art in the delivery of photosensitizers for photodynamic therapy. *Journal of Photochemistry and Photobiology B-Biology*, *66*(2), 89–106.

Lee, S. J., Park, K., Oh, Y. K., Kwon, S. H., Her, S., Kim, I. S., Choi, K., Kim, H., Lee, S. G., Kim, K., & Kwon, I. C. (2009). Tumor specificity and therapeutic efficacy of photosensitizer-encapsulated glycol chitosan-based nanoparticles in tumor-bearing mice. *Biomaterials*, *30*(15), 2929–2939.

Li, F., Bae, B. C., & Na, K. (2010). Acetylated hyaluronic acid/photosensitizer conjugate for the preparation of nanogels with controllable phototoxicity: Synthesis, characterization autophotoquenching properties, and in vitro phototoxicity against He La cells. *Bioconjugate Chemistry*, *21*(7), 1312–1320.

Li, L., Huh, K. M., Lee, Y. K., & Kim, S. Y. (2010). Design of a multifunctional heparin-based nanoparticle system for anticancer drug delivery. *Macromolecular Research*, *18*(2), 153–161.

Li, L., Moon, H. T., Park, J. Y., Heo, Y. J., Choi, Y. D., Tran, T. H., Lee, Y. K., Kim, S. Y., & Huh, K. M. (2011). Heparin-based self-assembled nanoparticles for photodynamic therapy. *Macromolecular Research*, *19*(5), 487–494.

Linhardt, R. J. (1991). Heparin - an important drug enters its 7th decade. *Chemistry & Industry*, *2*, 45–50.

Liu, Z. H., Jiao, Y. P., Wang, Y. F., Zhou, C. R., & Zhang, Z. Y. (2008). Polysaccharides-based nanoparticles as drug delivery systems. *Advanced Drug Delivery Reviews*, *60*(15), 1650–1662.

MacDonald, I. J., & Dougherty, T. J. (2001). Basic principles of photodynamic therapy. *Journal of Porphyrins and Phthalocyanines*, *5*(2), 105–129.

Matsumura, Y., & Maeda, H. (1986). A new concept for macromolecular therapeutics in cancer chemotherapy: Mechanism of tumoritropic accumulation of proteins and the antitumor agent smancs. *Cancer Research*, *46*(12, Pt 1), 6387–6392.

Mousa, S. A., & Petersen, L. J. (2009). Anti-cancer properties of low-molecular-weight heparin: Preclinical evidence. *Thrombosis and Haemostasis*, *102*(2), 258–267.

Park, I. K, Kim, Y. J., Tran, T. H., Huh, K. M., & Lee, Y. K. (2010). Water-soluble heparin-PTX conjugates for cancer targeting. *Polymer*, *51*(15), 3387–3393.

Park, I. K., Tran, T. H., Oh, I. H., Kim, Y. J., Cho, K. J., Huh, K. M., & Lee, Y. K. (2010). Ternary biomolecular nanoparticles for targeting of cancer cells and anti-angiogenesis. *European Journal of Pharmaceutical Sciences*, *41*(1), 148–155.

Park, K., Lee, G. Y., Kim, Y. S., Yu, M., Park, R. W., Kim, I. S., Kim, S. Y., & Byun, Y. (2006). Heparin-deoxycholic acid chemical conjugate as an anticancer drug carrier and its antitumor activity. *Journal of Controlled Release*, *114*(3), 300–306.

Roder, B., Hanke, T., Oelckers, S., Hackbarth, S., & Symietz, C. (2000). Photophysical properties of pheophorbide a in solution and in model membrane systems. *Journal of Porphyrins and Phthalocyanines*, *4*(1), 37–44.

Roslaniec, M., Weitman, H., Freeman, D., Mazur, Y., & Ehrenberg, B. (2000). Liposome binding constants and singlet oxygen quantum yields of hypericin, tetrahydroxy helianthrone and their derivatives: Studies in organic solutions and in liposomes. *Journal of Photochemistry and Photobiology B-Biology*, *57*(2–3), 149–158.

Smorenburg, S. M., & Van Noorden, C. J. F. (2001). The complex effects of heparins on cancer progression and metastasis in experimental studies. *Pharmacological Reviews*, *53*(1), 93–105.

Tang, P. M., Chan, J. Y., Au, S. W., Kong, S. K., Tsui, S. K., Waye, M. M., Mak, T. C., Fong, W. P., & Fung, K. P. (2006). Pheophorbide a, an active compound isolated from *Scutellaria barbata*, possesses photodynamic activities by inducing apoptosis in human hepatocellular carcinoma. *Cancer Biology & Therapy*, *5*(9), 1111–1116.

Tang, P. M., Liu, X. Z., Zhang, D. M., Fong, W. P., & Fung, K. P. (2009). Pheophorbide a based photodynamic therapy induces apoptosis via mitochondrial-mediated pathway in human uterine carcinosarcoma. *Cancer Biology and Therapy*, *8*(6).

Thunberg, L., Backstrom, G., Wasteson, A., Robinson, H. C., Ogren, S., & Lindahl, U. (1982). Enzymatic depolymerization of heparin-related polysaccharides. Substrate specificities of mouse mastocytoma and human platelet endo-beta-D-glucuronidases. *Journal of Biological Chemistry*, *257*(17), 10278–10282.

Yin, X., Zhou, J., Jie, C., Xing, D., & Zhang, Y. (2004). Anticancer activity and mechanism of *Scutellaria barbata* extract on human lung cancer cell line A549. *Life Science*, *75*(18), 2233–2244.